To be Published as: Protection of our cultural heritage: Examination of bending issues during the preservation of wall-paintings.

By: Advanced Nondestructive and Structural Techniques for Diagnosis, Redesign and Health Monitoring for the Preservation of Cultural Heritage: Selected work from the TMM-CH2023, A Springer book series Springer Proceedings in Materials. Springer Nature Switzerland AG

Protection of our cultural heritage: Examination of bending issues during the preservation of wall-paintings

Angelos Ntaflos[0000-0002-7212-4446]a, Maria-Elissavet Kouli[0000-0145-1908-1408] a, Alexandra Papapavlou[0000-0001-7691-291X] a, Christina Gioti[0000-0003-3832-947X]a, Maria Kosarli[0000-0001-5998-695X]a, Alkiviadis S. Paipetis[0000-0001-9668-9719]a,*

[a] Department of Materials Science and Engineering, University of Ioannina, 45110 Greece
*paipetis@uoi.gr

Abstract. Two wall paintings from the 19th century that were extracted from two different neo-classical mansions at Ioannina, Greece, were examined. In the second wall painting, a bending phenomenon was observed after the utilization of the framing protocol during the preservation process. The specimens were studied with an integrated approach, combining stoichiometric, and spectroscopic techniques. Spectral profiling techniques were used as a first step in evaluating the composition variation between the two paintings. Computed Tomography was employed (μCT) for the examination of the structure of the substrate. Results indicated that the absence of reinforcement inside the second wall painting as well as the poor diffusion of the materials used for the preservation process was the primary cause for bending.

Keywords: wall-painting, preservation, μCT.

1 Introduction

Cultural heritage artefact preservation is an integral part of archeology. Conservation techniques are being constantly improved for the optimal preservation of cultural heritage artefacts. Non-destructive evaluation techniques (NDT) are well-known for their ability to inspect and collect data from a structure or a material without damaging it. They are commonly used for the examination of cultural heritage objects since the evaluation of their condition must be performed without any intervention on their structure. The evaluation and identification of the materials of an artefact is fundamental for the design of a preservation or restoration strategy.

Fourier-transform infrared (FTIR) spectroscopy and Raman spectroscopy are widely used in the characterization of wall paintings, artefacts, artistic techniques, and generally in objects associated with cultural heritage. Both methodologies are non-destructive and qualitative and require a small sample for the analysis. The resulting spectrum represents a molecular fingerprint of the sample and can lead to the identification of the materials that are included. Laura Rampazzi used FTIR to identify aragonite and unusual pigments in 16th Century wall paintings (1). X-ray micro-Computed Tomography (μCT) has been increasingly used in the fields of cultural heritage and archeology for its ability to evaluate the microstructure of the material (2). A 3D full-volume

inspection of the sample can provide useful information about the microstructure such as volumetric data, porosity, density fluctuations, and hidden micro-defects. One of the most important advantages of μCT is the potential to share digital data, allowing easier dissemination and reducing the risk of damage (3).

Two wall paintings were restored by professional conservators with standard techniques and compatible materials, simulating the mortars used by builders during the 19th century. In this research, spectral and microscopic techniques have been implemented for the examination of the two paintings. The campaign was designed to ascertain the cause of structural deformation on one of the paintings after restoration i.e to explore the mechanisms that caused a bending phenomenon during the framing process. More specifically, two wall paintings from two different 19^{th}-century neo-classical mansions at Ioannina, Greece were examined. The first painting (hereafter referred to P1) was examined as a reference. The second one (hereafter referred to as P2) exhibited a bending phenomenon as well as crack failure. The two paintings underwent a typical restoration process from the professionals that involved (i) the removal from the wall, (ii) rinsing with water and ethanol, (iii) coating with Primal acrylic paint for consolidation of the plaster and curing for 24 hours, (iv) attachment on a framed canvas with a vinyl-based adhesive (Vinavil) and mortar mixture and (v) drying in room temperature. Upon the end of the process, it was observed that P2 exhibited bending which caused its surface to curve outwards and fracture. The performed analysis aimed at identifying the causes of this bending that ultimately led to the damage of the second painting, both in terms of the materials involved in the restoration process and in terms of the resulting microstructure.

2 Materials & Methods

2.1 Materials

For both paintings, samples were extracted from the surface painted layer ($P1_Z$, $P2_Z$) and from the substrate plasters (bonding material with the wall) ($P1_K$, $P2_K$) as can be seen in Figure 1.

Fig. 1: Designation of samples.

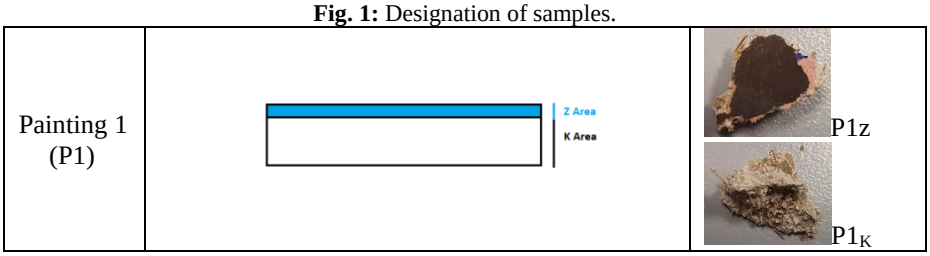

Painting 2 (P2)		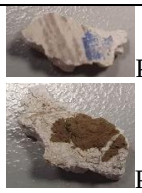 P2z P2$_K$

2.2 X-Ray Diffraction (XRD)

The X-ray powder diffraction patterns of the materials were collected on a D8 Advance Bruker diffractometer using Cu Ka (40 kV, 40 mA, λ = 1.541 78 Å) radiation and a secondary beam graphite monochromator (measurement conditions: 2θ = 10–80 degrees, in steps of 0.02 degrees and 2 s counting time per step).

2.3 Raman spectroscopy

Raman spectroscopy was employed using a Labram HR – Horiba confocal Raman microscope. A diode laser operating at 784 nm was used for the excitation of the Raman activity with 1 mW at the focal plane. An optical microscope with a 50 × objective was used both for laser delivery and for the collection of the Raman back-scattered light. Raman spectra were acquired in the range of 100–3500 cm^{-1}.

2.4 Fourier Transform InfraRed spectroscopy-FTIR

Infrared (FT-IR) spectroscopy was performed on powdered samples dispersed in KBr pellets with a JASCO FT/IR-6000 Fourier Transform spectrometer. The obtained spectra were averaged over 32 scans at 4 cm^{-1} resolution in the wavenumber range of 400–4000 cm^{-1}.

2.5 Micro-computed tomography (µCT)

The X-ray micro-computed tomography was used for the examination of the internal structure of the two paintings. A 3D X-ray microscope SKYSCAN 1275 by Bruker SA was used. The X-ray Source had a range of 40-100 kV. Reconstruction and analysis of the paintings were performed in the appropriate software by Bruker SA.

3 Results

3.1 XRD

Figure 2 (left) presents the XRD spectra of P1$_Z$ and P2$_Z$. Both XRD patterns were very similar with several mineral phases being observed. As shown, calcite was the main phase identified, followed by dolomite, gypsum, and quartz, confirming the results of Raman and FTIR spectroscopies presented after. Figure 2 (right) depicts the XRD

spectra of $P1_K$ and $P2_K$ samples. Both XRD patterns were very similar to the previous. As was observed, calcite was the main phase identified, followed by dolomite and quartz. However, in the $P2_K$ sample manganite and another form of calcium carbonate, aragonite, were observed.

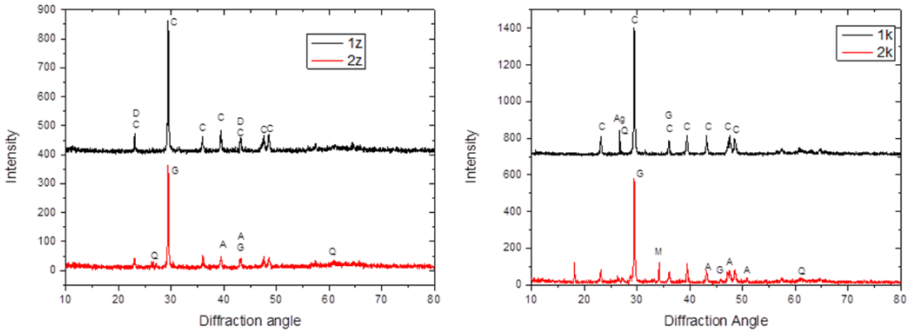

Fig. 2. XRD spectra of $P1_Z$ and $P2_Z$ samples (left) and $P1_K$ and $P2_K$ samples (right). C=Calcite, D=Dolomite, Q= Quartz, G=Gypsum, M= Manganite, Ag= Ag2O3, A=Aragonite.

3.2 Raman Spectroscopy

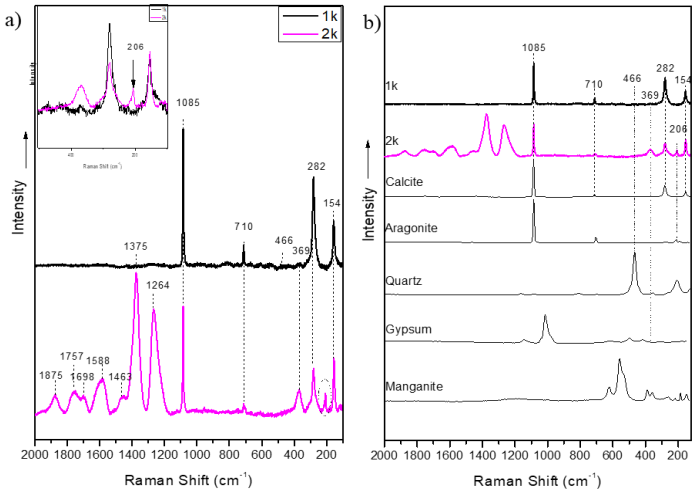

Fig. 3. (a) Raman spectra of $P1_K$ and $P2_K$ samples, **(b)** Raman spectra of P1K and $P2_K$ samples in comparison to crystalline phases detected through XRD.

Figure 3(a) presents the Raman spectra of $P1_K$ and $P2_K$ samples from P1 and P2 respectively. Table 1 presents the peak assignment and detailed information about the vibrational modes based on the bibliography. It is obvious that both samples showed similar spectral features until certain frequencies, which can be mainly attributed to calcite (4). Also, both spectra exhibit a band at 369 cm^{-1}, which was relatively weak for the $P1_K$,

while seems to be more intense at the $P2_K$ spectrum and can be possibly rendered to more gypsum existence in the $P2_K$ (5,6). On the other hand, the two spectra exhibited certain differences at low frequencies, such as the low intense peak 206 cm^{-1} (from the aragonite (7)) at the $P2_K$ (figure 3a- inset magnified region) which was absent at the $P1_K$. Also, in the $P1_K$, the low intense band at 466 cm^{-1} was attributed to quartz but did not appear in the $P2_K$. However, it is obvious that the main differences of the samples were those displayed at high frequencies for the $P2_K$. Those bands can be attributed to egg white, which according to literature was commonly used as a binder (8), or to casein, an ingredient extracted from cow's milk (9). The analyzed results of the Raman spectra of the $P1_K$ and $P2_K$ were in good agreement with XRD. Additionally, in figure 3(b) the crystalline phases of calcite, aragonite, quartz, gypsum, and manganite along with $P1_K$ and $P2_K$ spectra are presented, for optical investigation. It is clear that the characteristic peaks of the spectra correspond to the phases referred to above.

Table 1. Raman Peak Analysis differences between P1K and P2k samples

Frequency Shift (cm^{-1})	**P1K**	**P2k**	**Assingment**	**Crystal polymorphs**
206	-	✓	Symmetric single degenerate (7)	Aragonite
466	✓	-	Symmetric stretching vibrations of Si-O-Si bonds(10,11)	Quartz
1264	-	✓	Amide III (8)	Egg white
1375	-	✓	Bending (deformation vibrations of methyle group-CH_2, $\delta(CH_3)$ (8)	Egg white
1463	-	✓	Bending (deformation vibrations of methylene group-CH_2) (8)	Egg white
1588	-	✓	Stretching vibrations (Amide I) (12)	Casein
1698	-	✓	Stretching vibrations of the (C=O) peptidic bonds of Amide I (8), (12)	Egg white/ Casein
1757	-	✓	v(C=O) fatty acid esters (8)	Egg white

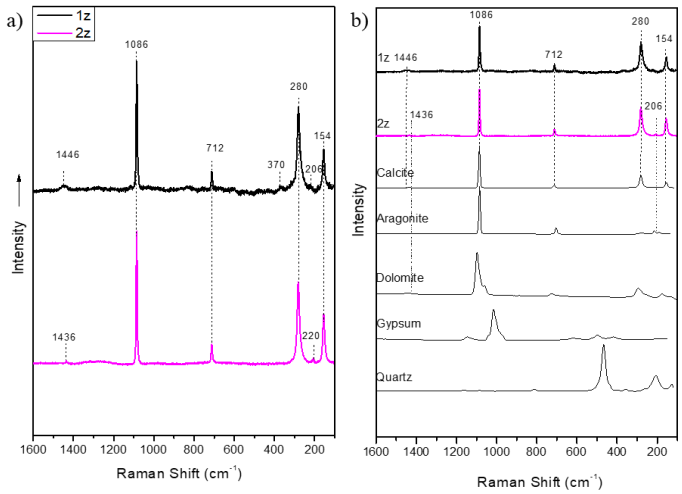

Fig. 4. (a) Raman spectra of P1z and P2z samples, **(b)** Raman spectra of P1z and P2z samples in comparison to crystalline phases detected through XRD.

Samples P1z and P2z come from the painting substrate of the wall paintings. The two spectra are identical (figure 4a), except from some slight differences. Peaks that correspond to aragonite appear also in these samples, at 206 cm^{-1} for the $P1_Z$ sample and slightly displaced at 220 cm^{-1} for the $P2_Z$ sample respectively. The broad band at 1446 cm^{-1} corresponds to calcite, while the band at 1436 cm^{-1} can be possibly attributed to dolomite [10]. Table 2 presents the peaks assignment and the vibrational modes differences between the two samples based on the bibliography. The Raman analysis of the 1Z and 2Z samples are in good agreement with XRD as previously. Figure 4(b) presents the crystalline phases detected with XRD for comparison with the P1z and P2z samples.

Table 2: Raman Peak Analysis differences for P1z and P2z samples

Frequency Shift (cm^{-1})	P1z	P2z	Assignment	Crystal polymorphs
1436	-	✓	Asymmetric stretching modes $(CO_3)^{2-}$ (13)	Dolomite
1446	✓	-	Asymmetric stretching modes $(CO_3)^{2-}$ (13)	Calcite

3.3 FTIR

Mid-IR spectra of $P1_K$ and $P2_K$ demonstrate several bands that appeared in both samples [Figure 4(a)]. In Table 3 the peak assignment and the vibrational modes are illustrated. The characteristic bands of calcite are present, in good agreement with Raman spectra (14). Also, both samples show low intense bands at 1027 cm^{-1} and 1631 cm^{-1} as well as a broad peak at 3434 cm^{-1} in both samples which were assigned to gypsum (15).

However, the two spectra exhibited certain differences, such as the additional low-intensity sharp band at 852 cm^{-1} and a small shoulder at 1489 cm^{-1}, observed in the $P2_K$ sample, which was probably due to an additional form of calcium carbonate, aragonite (16). Figure 4(b) provides a comparison among the $P1_K$ and $P2_K$ spectra with crystalline phases detected through XRD.

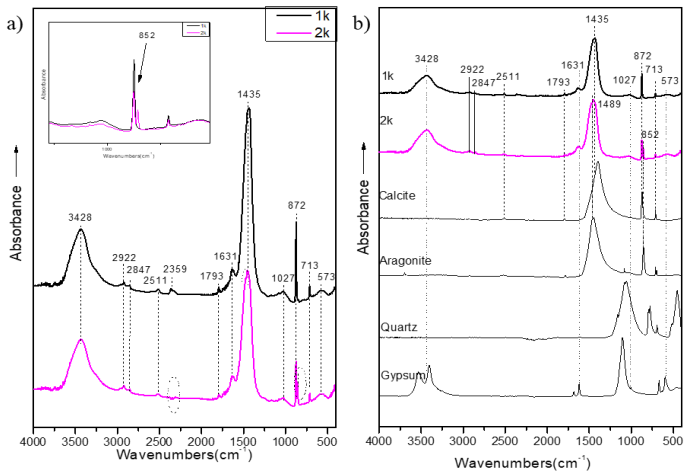

Fig. 5. (a) FT-IR spectra of $P1_K$ and $P2_K$ samples, **(b)** FT-IR of $P1_K$ and $P2_K$ samples in comparison to crystalline phases detected through XRD.

Table 3: Mid- Infrared Peak Analysis for P1K and P2k samples

Frequency Shift (cm^{-1})	$P1_K$	$P2_K$	Assignment	Crystal polymorphs
852	-	✓	Out of plane bending vibrations (16)	Aragonite
1489	-	✓	C-O bending modes (17)	Calcite

The $P1_Z$ and $P2_Z$ originate from the painting substrate of the wall paintings and also exhibit bands attributed to calcite and aragonite (figure 6a). The area both mansions are build is a high-humidity environment that favors the formation of natural aragonite (18).

The only difference presented was the low intense band at 852 cm^{-1} at the $P2_Z$ sample, which is attributed to the silicate phase of dolomite (19) and was absent in the P1z spectrum. Table 4 presents the characteristic peaks of the spectra. However, even though the XRD did not show gypsum existence in the $P1_Z$, infrared peaks at 1631 cm^{-1} and 2515 cm^{-1} could possibly be rendered to gypsum (15). The assignment of the absorption bands analyzed before is more obvious in figure 6b. It is also important to pinpoint that the mid-IR analysis was in good agreement with Raman spectroscopy.

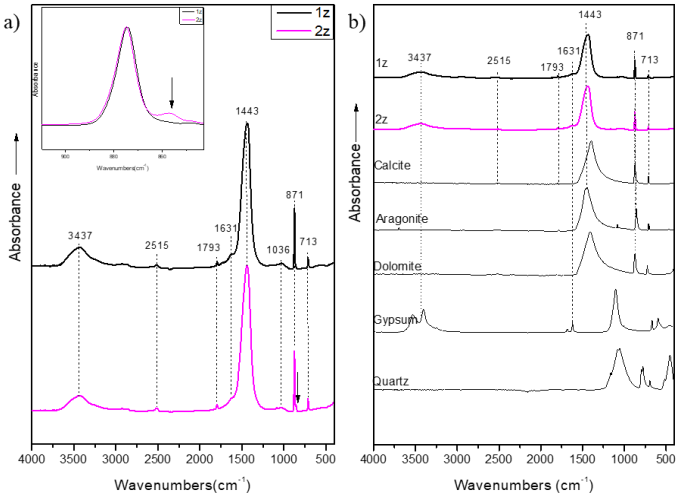

Fig. 6. (a) Mid-IR spectra of P1z and P2z samples, (b) Mid-IR spectra of P1z and P2z samples in comparison to crystalline phases detected through XRD.

Table 4. Mid- Infrared Peak Analysis differences between P1z and P2z samples

Frequency Shift (cm^{-1})	P1z	P2z	Assignment	Crystal polymorphs
852	-	✓	Si-O vibration of the silicate phase (19)	Dolomite
1793	-	✓	Symmetric stretching vibration (CO_3) (20)	Calcite

3.4 Micro-CT

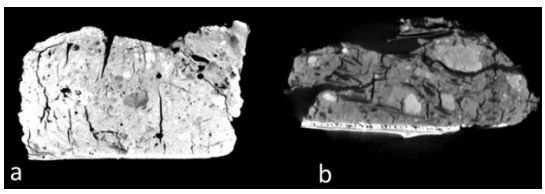

Fig.7. a) µCT slice of "WP 1", b) µCT slice of "WP 2".

Figure 7 shows CT images of the two wall-paintings (containing both the painted layers and the plaster substrate) obtained at 40 kV.The structure, from pores or internal defects (black areas) and the mortar (white areas), are clearly visible. The reconstruction of the raw µCT data was performed in Nrecon software. Slices of the materials were extracted, and qualitative analysis was performed in CTAn software. A representative region of interest (ROI) of 3 mm^3 was selected for both samples due to their geometrical anisotropy (Figure 8). Binary images were obtained to extract information about the porous volume after filtering with a gaussian filter and thresholding using integrated plug-ins of the CTAn software. The porosity of each sample was measured per CT slice and for

the selected volume of interest as a whole. The P2 sample had a total porosity of 7 % compared to the 22 % of the P1 The structure of the two paintings differs due to the inclusion of natural fibers as a reinforcing agent in P1

During the preservation process, at the third step, a coating of Primal acrylic paint and then a mixture of Vinavil and mortar were applied to consolidate and strengthen the initial substrate of the painting. The applied adhesion to P1 was successful due to the higher porosity since the mixture was able to diffuse into the pores of the structure evenly. As observed by other researchers, the addition of fibers in mortars absorb part of the transformation energy and contributes to volume stability as they don't permit the collapse of the structure after the application of load (21). Other researchers report that fibers increase flexural strength from bending tests as much as 100% compared to plain mortars (22).

In contrast, P2 had low porosity due to its different microstructure. The absence of fibers could also affect the stiffness of the material. As observed by the preservation team the consolidant did not diffuse evenly into the substrate. Upon the hydration of the mortar/Vinavil mixture, the uneven distribution of the Primal caused differential strains at random sites and ultimately bending and microcracking.

Fig. 8. Regions of interest of the two samples.

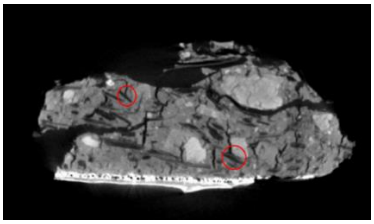

Fig. 9. Fibers introduce crack deflection mechanisms in the mortars.

4 Conclusions

Two wall paintings were compared in their structure and materials since one of them was damaged during its preservation process. The first painting was used as a reference since it was not affected by the preservation process. A bending phenomenon was observed during the framing protocol of the second painting when followed by the conservators. A complete characterization of the materials included in the substrate of the painting was performed using a variety of NDE techniques to identify any differences in their structure. Micro-CT (μCT) was used for the evaluation of the internal structure and porosity of the samples.

Information extracted through vibrational spectroscopies provided a clear view of the materials included in the two samples. Vibrational Spectroscopies (Raman and mid-IR) and XRD revealed almost identical spectra, with certain differences in some of the materials included such as the existence of egg white. The P2 contained more gypsum in its structure as confirmed by FTIR, Raman, and XRD. These differences may affect the stiffness of the material as well as its strength.

After μCT characterization of the two samples, it was observed, that P2 which was damaged, did not have any reinforcing materials (natural fibers, etc.) in its structure. The absence of any reinforcement led to bending and failure since the painting could not sustain the load from the shrinkage of the mortar mixture placed during the framing protocol.

5 Acknowledgments

We acknowledge support of this work by the project “Center for Research, Quality Analysis of Cultural Heritage Materials and the Communication of Science” (MIS5047233) which is implemented under the Action “Reinforcement of the Research and Innovation Infrastructure”, funded by the Operational Programme "Competitiveness, Entrepreneurship and Innovation" (NSRF 2014-2020) and co-financed by Greece and the European Union (European Regional Development Fund).

6 References

1. Rampazzi L, Corti C, Geminiani L, Recchia S. Unexpected findings in 16th century wall paintings: Identification of aragonite and unusual pigments. Heritage. 2021 Sep 1;4(3):2431–48.
2. Sodini N, Dreossi D, Chen R, Fioravanti M, Giordano A, Herrestal P, et al. Non-invasive microstructural analysis of bowed stringed instruments with synchrotron radiation X-ray microtomography. J Cult Herit. 2012;13(3 SUPPL.):S44–9.
3. Methods A, Amctb C. X-ray micro computed tomography in cultural heritage. Analytical Methods. 2020;12(36):4496–500.
4. Buzgar N, Apopei AI. The Raman study of certain carbonates. Geologie Tomul L. 2009;2(2):97–112.
5. Sarma LP, Prasad PSR, Ravikumar N. Raman spectroscopic study of phase transitions in natural gypsum. Journal of Raman spectroscopy. 1998;29(9):851–6.
6. Prieto-Taboada N, Gomez-Laserna O, Martinez-Arkarazo I, Olazabal MÁ, Madariaga JM. Raman spectra of the different phases in the CaSO4–H2O system. Anal Chem. 2014;86(20):10131–7.
7. De La Pierre M, Carteret C, Maschio L, André E, Orlando R, Dovesi R. The Raman spectrum of CaCO3 polymorphs calcite and aragonite: a combined experimental and computational study. J Chem Phys. 2014;140(16):164509.

8. Osticioli I, Nevin A, Anglos D, Burnstock A, Cather S, Becucci M, et al. Micro-Raman and fluorescence spectroscopy for the assessment of the effects of the exposure to light on films of egg white and egg yolk. Journal of Raman Spectroscopy. 2008;39:307–13.
9. Hajjia S, Turkia T, Boubakric A, Amora M Ben, Mzoughid N. Study of cadmium adsorption onto calcite using full factorial experiment design. In: Presented at the 5th Maghreb Conference on Desalination and Water Treatment—CMTDE. 2015.
10. Sharma S, Misra A, Ismail S, Singh U. Remote Raman Spectroscopy of Various Mixed and Composite Mineral Phases at 7.2 m Distance. 2006;
11. KRISHNAN RS. Raman Spectrum of Quartz. Nature. 1945;155(3937):452.
12. Wang J, Su Y, Jia F, Jin H. Characterization of casein hydrolysates derived from enzymatic hydrolysis. Chem Cent J. 2013;7(1):1–8.
13. Gunasekaran S, Anbalagan G. Thermal decomposition of natural dolomite. Bulletin of Materials Science. 2007;30(4):339–44.
14. Reig FB, Adelantado JVG, Moreno MCMM. FTIR quantitative analysis of calcium carbonate (calcite) and silica (quartz) mixtures using the constant ratio method. Application to geological samples. Talanta. 2002;58(4):811–21.
15. Anbalagan G, Mukundakumari S, Murugesan KS, Gunasekaran S. Infrared, optical absorption, and EPR spectroscopic studies on natural gypsum. Vib Spectrosc. 2009;50(2):226–30.
16. Chakrabarty D, Mahapatra S. Aragonite crystals with unconventional morphologies. J Mater Chem. 1999;9(11):2953–7.
17. Al Dabbas M, Eisa MY, Kadhim WH. Estimation of gypsum-calcite percentages using a Fourier transform infrared spectrophotometer (FTIR), in Alexandria Gypsiferous Soil-Iraq. Iraqi J Sci. 2014;55(4B):1916–26.
18. Frankeová D, Koudelková V. Influence of ageing conditions on the mineralogical micro-character of natural hydraulic lime mortars. Constr Build Mater. 2020 Dec 20;264.
19. Karimi Shahraki B, Mehrabi B, Dabiri R. Thermal behavior of Zefreh dolomite mine (Central Iran). Journal of Mining and Metallurgy, Section B : Metallurgy. 2009;45.
20. Rodriguez-Blanco J, Shaw S, Benning L. The Kinetics and Mechanisms of Amorphous Calcium Carbonate (ACC) Crystallization to Calcite, Via Vaterite. Nanoscale. 2010;3:265–71.
21. Stefanidou M, Papachristoforou M, Kesikidou F. Fiber-reinforced lime mortars. 2016.
22. DRDACKY MF, Dagmar MICHOINOVA. LIME MORTARS WITH NATURAL FIBRES. Brittle Matrix Composites 7. 2003;515–21.